ORIGINAL ARTICLE

The characteristics of blasting vibration frequency bands in jointed rock mass slope

Shenghui Zhang[1] · Wenxue Gao[1] · Lei Yan[2] · Jiangchao Liu[1] · Liansheng Liu[2]

Abstract

High-slope and rock mass joint development are the factors for predicting and controlling blasting vibrations under open pit mining. Blasting vibration adversely affects the stability of jointed rock slopes, thus studying the characteristics of blasting vibration frequency bands in jointed rock masses slope is an important task to ensure the safety of blasting operations. In the present study, vibratory ground motions were measured during blasting excavation in open-pit mining, and the blasting vibration frequency band characteristics of jointed rock masses and high slope were studied through the wavelet transform and response spectrum method. The results demonstrated that the amplification effects of the peak particle velocity (PPV) and energy between different frequency bands exhibited distinguishing characteristics. It was found that, with the increase in elevation, the PPV and energy amplification effects were the most obvious in the 0–16 Hz band, while they were attenuated in the 32–64 Hz band. Furthermore, the distribution of dominant frequency bands of vibration signals observed to be low and narrow, and the average frequency had been reduced. In the development of joints in rock masses, the PPV and energy in each frequency band were attenuated, and the distribution of the dominant frequency bands of vibration signals was high and wide. Also, the average frequency had been increased and the multi-modal characteristics of the responses to blasting vibrations were more obvious. The rock mass structures had displayed different amplification effects on the frequency components of the blasting seismic waves. Finally, as the effects of jointed rock masses on the blasting load responses could not be simply considered as reducing vibrations, they must be analyzed using vibration theory and actual situations.

List of symbols

$\ddot{x}$	Acceleration of the rock mass element
$\dot{x}$	Velocity of the rock mass element
x	Displacement of the rock mass element
ω	Excitation frequency
ω_0	Natural frequency of the slope
ζ	Damping ratio
c	Viscous damping coefficient
m	Mass of the rock mass element
t	Time
τ	Specific time
v_0	Initial velocity
d_0	Initial displacement
I	Instantaneous impulse
p	Blasting load
$d\tau$	Micro-segment
dt	Time step-size
dx	Displacement step-size
$\psi(t)$	Arbitrary signal
$L^2(R)$	A signal space with limited energy
R	Real number
$\hat{\psi}(\omega)$	Fourier transformed arbitrary signal
C_ψ	Permitted condition
f	Function
$W_f(a, b)$	The continuous wavelet transform for any function
a	Scaling factor
b	Translation factor
Z	Natural number
i	Specific natural number
j	Specific natural number
k	Specific natural number

✉ Liansheng Liu
liulsjxust@163.com

1 College of Architecture and Civil Engineering, Beijing University of Technology, Beijing 100124, China

2 School of Resource and Environmental Engineering, Jiangxi University of Science and Technology, Ganzhou 341000, China

Δa	Scale interval
Δb	Time interval
E	Energy
η	Relative energy
$\bar{f}$	Average frequency
f_i	Each frequency in the Fourier Spectrum
A_i	Amplitude associated with each frequency

Introduction

Explosive fragmentation along high rock slopes in open pit mines produces adverse effects (Tuckey and Stead 2016; De 2012; Wang and Shukla 2010; Park et al. 2009). These effects are predominantly the result of vibratory ground motions (Mohammadnejad et al. 2012; Ghoraba et al. 2016; Hosseini et al. 2019). If the vibration intensities exceed the resistance of the protected objects, then they may be damaged (Xue and Yang 2014; Zhou et al. 2016). Blasting vibrations may also reduce the stability of high slopes (Salvoni and Dight 2016), through local cracking, loosening, and slippage of the rock masses, which could lead to collapse and landslides (Xu et al. 2016; Nie et al. 2015; Herrera et al. 2010). Havenith et al. (2003) used a finite element method for the numerical simulations of landslide response characteristics. The results indicated that the strain localization was closely related to the wave amplification in the surficial low-velocity layers, especially below the convex surface morphologies. Graizer (2009) found that the low-velocity rock layers and geomorphology lead to local amplification effects. Hu et al. (2017) proposed the concept of equivalent paths and distances in open pit slopes under the influences of multiple factors. The resulting formula for the relationship between the PPV and the equivalent distance, included topography effects on attenuation. Chen et al. (2011) studied the effects elevation amplification of particle velocities on slopes based on a static theory, numerical simulations, and field experiments. It was found that "whiplash effects" had been caused in the rock structures of slope benches and the vibrations were observed to be amplified, particularly at the edges of the benches. Hu et al. (2018) studied the relationship between the damage depths and the PPV through experiments and simulations, and introduced an equivalent blasting vibration control standard (EBVCS) which proposed a damage-vibration coupling control method for high rock slopes. Many previous research studies have introduced elevation to modify the Sadov Formula (Ghasemi et al. 2013; Torres et al. 2018; Jiang et al. 2017; Nateghi 2011), by means of applying multiple regression, and studied the attenuation law of blasting seismic waves to predict the vibration in specific engineering projects. However, the above-mentioned research studies mainly focused on the influences of topography and elevation on the propagation

law of blasting seismic waves. Therefore, the influences of rock masses with joints on the blasting vibrations in high slopes require further examination.

Rock masses are heterogeneous and anisotropic discontinuous structures which are quasi-randomly intersected by different types of planes of weakness, such as faults, joints, fracture zones, and so on. When blast seismic waves propagate through the jointed rock, the attenuation of blast vibration will be affected by the characteristics of the joint surfaces, as well as the rock wave impedance on both sides of each discontinuous surface, angles of the discontinuous surfaces, and direction of the propagation (Wu et al. 1988). In the current available related literature (Kumar et al. 2018; Farrokhi et al. 2016; Abdelwahed and Abdel-Fattah 2015; Wu and Aki 1988), it was found that the propagation characteristics of seismic waves in jointed rock masses have been extensively studied. It has been determined that after the seismic waves pass joints in rock masses, the attenuation of the transmitted wave amplitudes may be caused by two aspects. On one hand, the energy of the stress waves will dissipate as the waves pass through damped joints, which is referred to as intrinsic attenuation. On the other hand, when seismic waves pass through joints to generate transmitted waves and reflected waves, the stress wave energy will be transferred, which is referred to as form attenuation. Researchers have used 3DEC or UDEC simulation method to study the propagation characteristics of stress waves in jointed rock masses (Sebastian and Sitharam 2014; Deng et al. 2012; Li et al. 2011; Zhao et al. 2008; Fan et al. 2004; Nakagawa et al. 2000). Azizabadi et al. (2014) utilized waveform superposition and numerical simulations to calculate the effects of blasting vibrations on the stability of slopes in jointed rock masses. If there are joints in the excavation area of the rock mass, the blasting effects will be affected. Rathore and Bhandari (2007) were able to produce macroscopic cracks in desired directions by controlling blasting techniques, while protecting the development of cracks in the remaining rock. In a related study, Wang and Xiong (2020) studied the influence of the shear strength of jointed rock masses by setting bolts under different conditions. Bahrani and Kaiser (2013) studied the strength degradation of discontinuous rock masses by conducting laboratory tests on intact and discontinuous rock samples, which are known to be the main reasons why jointed rock masses are more easily damaged under blasting actions. The above-mentioned studies have made many contributions to the blasting seismic wave propagation law and blasting vibration control methods in jointed rock masses. However, it remains important to also study the blasting vibration frequency band characteristics of rock masses with joints.

In the excavation of some rock mass projects, encountering special geological conditions will cause difficulties to construction. Zhang et al. (2018) studied the stability of

horizontal rock strata in tunnel construction and Xue and Zhang (2020) studied the failure mode and stability of excavation face on shield tunnel undercrossing the existing tunnel. Their research has contributed to ensuring the safety and efficient construction of the project. Yin et al. (2018) and Yuan et al. (2018) found that the main vibration frequency range of rock masses blasting is 0–50 Hz, by means of on-site ground vibration monitoring. Forcellini et al. (2018) studied the response point analysis of the 3D homogeneous soil model, and considered different values of depth for each soil type and seismic intensity, so as to monitor their effects on the obtained results. Unfortunately, they did not consider the influence of rock masses with joints and high rocky slopes factors on the change of blasting vibration frequency band characteristics, and combined the relationship between excitation frequency and natural frequency to study the vibration response characteristics of jointed rock masses.
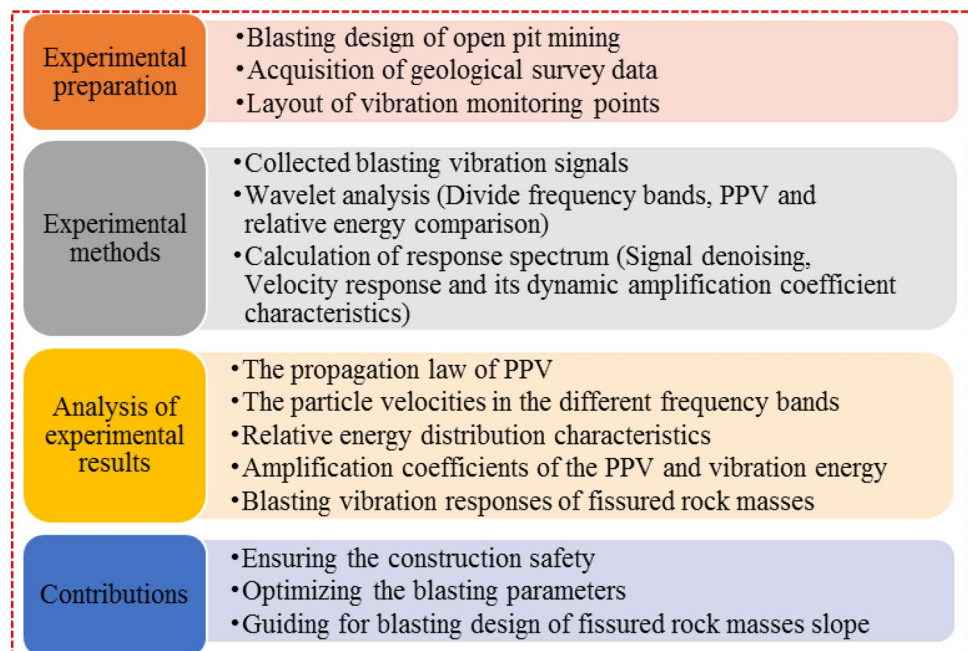
The present study aims to control and predict the blasting vibrations of rock masses with joints and high slopes. High-slope and rock masses joints development are the factors for predicting and controlling blasting vibrations under open-pit mining. With the increasing exploitation of open-pit mines, deep pits have been gradually formed, and the exposed final slopes are becoming increasingly higher and steeper. The responses of the jointed rock masses to the blasting vibrations were determined by the external loads and inherent characteristics of the rock structures. Therefore, the blast-induced vibration instability of the jointed rock masses will become more important as slope elevations increase. To reduce the impact of blasting vibration on the pre-reserved slope, studying the characteristics of blasting vibration frequency bands in jointed rock masses slope is an important task to ensure the safety of blasting operations. As illustrated in Fig. 1, first, blast-induced vibrations were measured in an open pit excavation site, and the law of PPV propagation on rock masses slope was studied. Next, a wavelet transform method was used to obtain the particle velocities and relative energy distribution characteristics of the blasting in different frequency bands, focusing on the analysis of the particle velocity and energy amplification effect in the main frequency bands. Finally, the relationship between the natural frequency and excitation frequency was investigated, and the response characteristics of jointed rock mass were analyzed based on a response spectrum calculation. It was expected that the results obtained in this study could potentially provide a guide for future blasting excavations of high rock slopes with joints.

Mechanical description of the blasting vibration intensities in the jointed rock masses

Analysis of the blasting vibration intensities of the rock masses involves wave propagation and vibration perspectives. The wave theory established the kinematic equations for the attenuation and dispersion of the blasting seismic waves based on the Huygens-Fresnel Principle and Snell Refraction Law (Shan et al. 2006). The vibration theory was able to describe the vibration response characteristics of the rock mass structures based on the D'Alembert Principle (Lv 2015). When studying the propagation characteristics of the

Fig. 1 Flowchart for this study

Experimental preparation	• Blasting design of open pit mining • Acquisition of geological survey data • Layout of vibration monitoring points
Experimental methods	• Collected blasting vibration signals • Wavelet analysis (Divide frequency bands, PPV and relative energy comparison) • Calculation of response spectrum (Signal denoising, Velocity response and its dynamic amplification coefficient characteristics)
Analysis of experimental results	• The propagation law of PPV • The particle velocities in the different frequency bands • Relative energy distribution characteristics • Amplification coefficients of the PPV and vibration energy • Blasting vibration responses of fissured rock masses
Contributions	• Ensuring the construction safety • Optimizing the blasting parameters • Guiding for blasting design of fissured rock masses slope

blasting seismic waves in a homogeneous continuum, the corresponding wave equation can be used to solve the vibration amplitudes of the particles. However, the wave propagates in anisotropic discontinuous rock masses with joints have been observed differ from that in an isotropic homogeneous continuum. Although the jointed rock mass structure is a multi-degree of freedom system, we can simplify it into a single degree of freedom (SDOF) system to study its response under the blasting load. Based on the D'Alembert Principle (Lv 2015), the vibration equation of the particle system was expressed as follows:

$$\ddot{x} + 2\omega\zeta\dot{x} + \omega^2 x = 0 \tag{1}$$

where ω denotes the excitation frequency and it was expressed as $\omega = \omega_0\sqrt{1 - \xi^2}$, in which ω_0 represents the natural frequency of the slope; the damping ratio $\zeta = \frac{c}{2m\omega_0}$; m is the mass of the rock mass element; c represents the viscous damping coefficient.

The general solution for Eq. (1) was as follows:

$$x_0(t) = e^{-\xi\omega t}(A\cos\omega_0 t + B\sin\omega_0 t) \tag{2}$$

Assuming that at time $t = 0$, the initial displacement $U(0) = d_0$, the initial velocity $\dot{U}(0) = v_0$, and the following formula was derived:

$$\begin{cases} A = d_0 \\ B = \dfrac{v_0 + \xi\omega d_0}{\omega_0} \end{cases} \tag{3}$$

Thus, the solution of Eq. (2) can be written as:

$$x_0(t) = e^{-\xi\omega t}\left(d_0\cos\omega_0 t + \frac{v_0 + \xi\omega d_0}{\omega_0}\sin\omega_0 t\right) \tag{4}$$

During the process of the damped vibration, the free vibrations of the particle system disappeared quickly. Deriving the vibration response of the SDOF damping system under the blasting load $p(t) = m\ddot{x}(t)$, in which $\ddot{x}(t)$ is irregular (see Fig. 9), and it is necessary to introduce instantaneous impulse $I = pdt$.

As shown in Fig. 2, under the action of instantaneous impulse I, the SDOF damping system will vibrate freely under the conditions of initial velocity $v_0 = I/m$ and initial displacement $d_0 = 0$. The displacement at any time t is:

$$x(t) = e^{-\xi\omega t} \cdot \frac{pdt}{m\omega_0}\sin\omega_0 t \tag{5}$$

Assuming that the load excited at time $t = \tau$ is $p(\tau)$, then the impulse formed in micro-segment $d\tau$ at this moment is $p(\tau) \cdot d\tau$, combined with Eq. (5), the vibration caused by this impulse at $t(t \geq \tau)$ can be written as:
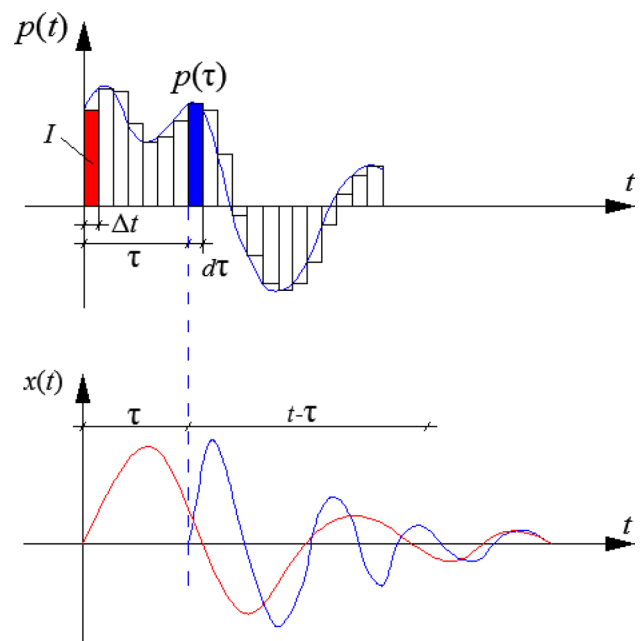

Fig. 2 Vibration response under blasting load

$$dx(t) = e^{-\xi\omega(t-\tau)} \cdot \frac{p(\tau)}{m\omega_0}\sin\omega_0(t - \tau)d\tau \tag{6}$$

Therefore, the relative displacement response of the SDOF damping system during the blasting load excitation process can be obtained:

$$x(t) = -\frac{1}{\omega_0}\int_0^t \ddot{u}_0(t) \cdot e^{-\xi\omega(t-\tau)} \cdot \sin\omega_0(t - \tau)d\tau \tag{7}$$

The derivative of Eq. (7) can obtain the velocity response of an SDOF damping mass system under blasting load, it has important theoretical significance and practical engineering value for studying the characterization of the vibration intensities in rock masses with joints and high slopes.

Material and methods

In the current study, vibratory ground motions were measured during blasting excavation of the open-pit slope of the Yongping Copper Mine in China's Jiangxi Province. The lithology in the study area was limestone inclusive with quartz sandstone, and the rock masses were observed to be relatively broken. Also, joints had developed which were filled with siliceous limestone and metallic minerals, with the majority being dry joints. Table 1 shows the mechanical properties of the investigated intact rock and jointed rock samples (Yongping Copper Mine Geology Department 2012), among which the existence of the rock mass joints

Table 1 Mechanical Properties of intact rock and jointed rock samples investigated (Source, Yongping Copper Mine Geology Department 2012)

Properties	Value of intact rock	Value of jointed rock
density	2680 kg m^{-3}	2610 kg m^{-3}
Elastic modulus	17.68 GPa	10.23 GPa
Compressive strength	67.68 MPa	36.87 MPa
Poisson's ratio	0.21	0.19
Cohesion	17.55 MPa	11.34 MPa
Internal friction angle	44.18°	37.22°
joint spacing	/	5–30 cm
joint aperture	/	0–2 cm

determines the nonlinearity, inhomogeneity, discontinuity, and anisotropy of the rock masses. The upper rock mass was a residual slope covered in very thick sediment, and the structures of the rock and soil layers were observed to be loose. The dip of the bedding planes in the lower rock layer ranged from 10° to 30°, and its dip direction was opposite to that of the slope. The details of the slope design are illustrated in Fig. 3.

This study's five monitoring points were arranged on the benches of the jointed rock masses with elevations of + 75 m (No. 1); + 95 m (No. 2); + 105 m (No. 3); + 115 m (No. 4); and + 135 m (No. 5), respectively. The distances from the monitoring points to the bottoms of the bench were approximately 3 m. In this study, CK914 and CK1101 represent geological exploration drilling numbers. The slope rock masses of the No. 2 (+ 95 m) and No. 4 (+ 115 m) benches had a wide range of tensile fracture zones. As detailed in Fig. 4, the joints of the rock masses on the No. 2 (+ 95 m) and No. 4 (+ 115 m) benches were developed, while those on the No. 1 (+ 75 m), No. 3 (+ 105 m), and No. 5 (+ 135 m) benches were relatively less.

The available devices of the Blast Mate III were able to record the particle velocities up to 254 mm/s, and sensors were installed on the surfaces of the rock masses for this study's experimental testing processes. Furthermore, several vibration tests were carried out on the row-by-row detonation millisecond delay blasts of the elevation + 55 m operational platform. A mixed emulsion explosive was used during the blasting operations. The density and detonation velocity of the explosive were 1.1 g/cm^3 and 3200 m/s, respectively. The diameter, depth, spacing, row spacing, and stemming length of the holes were 0.2 m, 11 m, 6.0 m, 5.0 m, and 5.0 m, respectively.

Fig. 3 The sectional view of the monitoring points arrangement. Noted: CK914 and CK1101 are geological exploration borehole numbers (Source, Yongping Copper Mine Geology Department 2012)
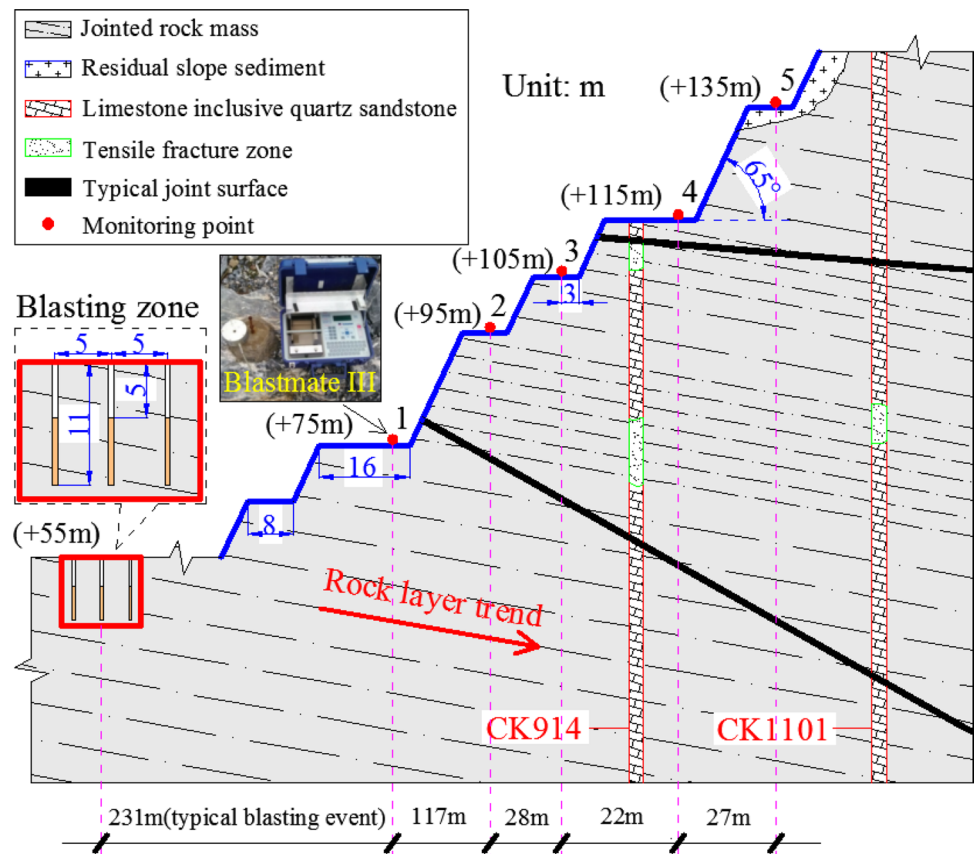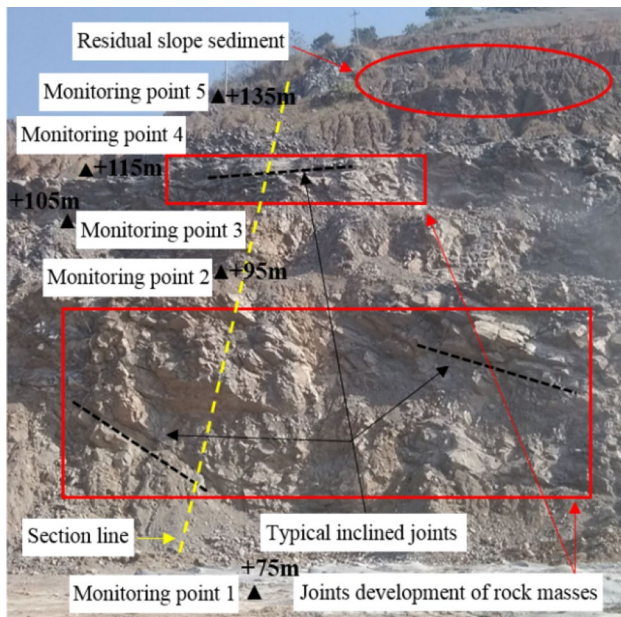
Fig. 4 Field investigation of slope jointed rock mass

Results

PPV for blasting events

As shown in Fig. 5, in many blasting events, the PPV of different elevation signals exhibits a relatively stable variation law on each component, and the PPV has certain elevation amplification effects. In the present study, under the influences of the joints in the rock masses, the peak particle velocities of Signal 2 (+95 m) and Signal 4 (+115 m) were found to be mainly attenuated. However, the PPV of Signal 4 (+115 m) was increased on the transversal component. This result may have been due to the fact that the elevation amplification effects had accounted for the main influence,

and also that the jointed rock mass structures had significantly responded to the blasting vibrations.

Comparative analysis of the PPV in the different frequency bands

A wavelet transform method (Cao and Guo 2016) is a time–frequency localization analysis method in which the window size is fixed. However, its shape, time window, and frequency window can be adjusted. This method allows resolution of frequencies with low time resolution for the low-frequency parts of signals, and also obtain higher time resolution with lower frequency resolution for the high-frequency parts of signals. Therefore, due to the high-frequency and low-frequency separation characteristics of wavelet transform methods, the signal characteristics of different scales can be characterized without losing the important information components of the original signal. To obtain useful signals, wavelet transform methods are widely applied in various fields, such as complex non-stationary signal processing, time–frequency analysis, and signal denoising.

It is known that the propagation of blasting seismic waves in the rock mass medium of the open-pit slope is affected by the characteristics of the explosive sources and the nature of the site. As a result, the velocities and energy levels between different frequency bands of blasting vibration signals tend to be different. In the present study, a wavelet transform method was used to separate the blasting vibration signals in a specific frequency range. However, the selection of the optimal wavelet base was especially critical. In previous studies, the Daubechies wavelet series (Yang et al. 2016; Huang et al. 2019) had achieved successful results in the analysis of non-stationary signal problems, including blasting vibration signals. However, db5 and db8 are currently most commonly used in blasting vibration signal analysis processes.
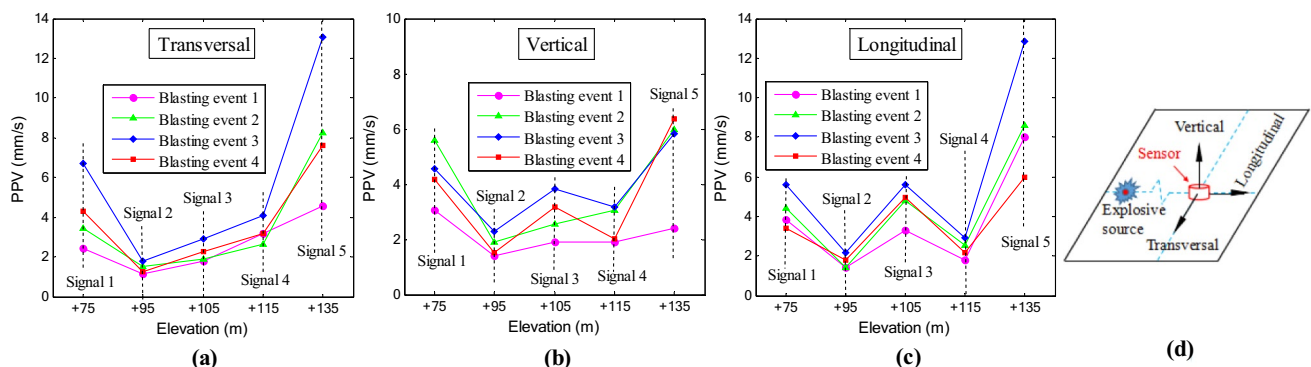

Fig. 5 The PPV for blasting events in different elevations: **a** transversal component; **b** vertical component; **c** longitudinal component; **d** three-dimensional coordinate components

In this study, based on the principle of wavelet transform (Cao and Guo 2016), and assuming $\psi(t) \in L^2(R)\,(L^2(R))$ is a signal space with limited energy, its Fourier transform can be written as $\hat{\psi}(\omega)$, if $\hat{\psi}(\omega)$ satisfies the following condition:

$$C_\psi = \int_R \frac{|\hat{\psi}(\omega)|^2}{|\omega|}d\omega < \infty \tag{8}$$

The continuous wavelet transform for any function $f(t) \in L^2(R)$ is as follows:

$$W_f(a,b) = |a|^{-\frac{1}{2}} \int_R f(t)\overline{\psi(\frac{t-b}{a})}dt \tag{9}$$

The continuous wavelet inverse transform is:

$$f(t) = \frac{1}{C_\psi} \int_{R^+} \int_R \frac{1}{a^2} W_f(a,b)\psi\left(\frac{t-b}{a}\right)dadb \tag{10}$$

where a and b are the scaling factor and translation factor, respectively, and $\overline{\psi\left(\frac{t-b}{a}\right)}$ is the conjugate function of $\psi\left(\frac{t-b}{a}\right)$.

Since the measured blasting vibration signals were composed of discrete data corresponding to a series of time sampling points, the parameters a and b needed to be discretized. These data need to be divided by a binary grid (for example: $a = 2^j, b = 2^j k,\ j, k \in Z$) to obtain the binary wavelet transform in the following formula:

$$W_{2^j}f(k) = 2^{-\frac{j}{2}} \int_R f(t)\overline{\psi(\frac{t}{2^j} - k)}dt \tag{11}$$

In many of the blasting vibration tests, a typical blasting event was selected. The total number of blast holes is 86, with 4 rows of holes, and the delay time of each row of holes is 75 ms. The single hole charge is about 200 kg, and the maximum explosive charge per delay is 4350 kg. Other parameters and monitoring results of the different measuring points are shown in Table 2 and Fig. 3. The sampling rate was 2048 Hz during the test, and the Nyquist frequency was 1024 Hz. The db8 (Yang et al. 2016; Huang et al. 2019) wavelet base was used to decompose the original signal of the measured Longitudinal component (Fig. 6) into six

levels. The division scale of the signal band was $a = 2^j$, and the first to seventh frequency bands were 0–16 Hz; 16–32 Hz; 32–64 Hz; 64–128 Hz; 128–256 Hz; 256–512 Hz; and 512–1024 Hz, respectively. Figure 6 presents the particle velocity time-history curve of the reconstructed seven frequency band signals.

The sum of the reconstructed signals which had been obtained by the wavelet transform method was in agreement with the measured original signal. However, it should be noted that signals had different vibration intensities in the different frequency bands. The particle vibration intensity of Signal 1 (+75 m) was mainly in the 16–32 Hz and 32–64 Hz bands. Also, it was observed to have a weak vibration amplitude in the 0–16 Hz and 64–128 Hz bands. It could be seen that as the elevation increased, the particle velocity of Signal 3 (+105 m) had increased and attenuated in the 0–16 Hz and 64–128 Hz bands, respectively. Furthermore, the particle velocity of Signal 5 (+135 m) had increased in the 0–16 Hz and 16–32 Hz band, while it was relatively weak in the 32–64 Hz band. Due to the development of joints in the rock masses of the No. 2 (+95 m) and No. 4 (+115 m) benches, the velocities in all frequency bands of Signal 2 (+95 m) and Signal 4 (+115 m) had displayed clear attenuations. However, they were found to have a lower attenuation rate in the 64–128 Hz band. The results demonstrated that the blasting vibration signals in the rock masses with joints of the slope had different frequency band characteristics.

Relative energy distribution characteristics of the vibration signals

The reconstructed waveform which was obtained by the wavelet transform showed that the particle velocities of the rock masses with joints at different elevations were different in each of the frequency bands. Therefore, to calculate the relative energy distribution characteristics between the different frequency bands of the signals, it should be pointed out that the relative energy of the signals was the percentage of the energy of specific frequency bands divided by that of all frequency bands (frequency range: 0–1024 Hz).

Table 2 Blasting parameters and measured data of monitoring points

| signals	Elevation (m)	Horizontal detonation distance (m)	PPV (mm/s)				Dominant frequency (Hz)		
			Transversal	Vertical	Longitudinal	Vector sum	Transversal	Vertical	Longitudinal
1	+75	231	4.318	4.191	3.429	5.647	29.88	29.31	29.63
2	+95	329	1.270	1.524	1.778	1.951	30.38	24.19	32.00
3	+105	355	2.286	3.172	4.953	5.385	18.13	23.88	18.13
4	+115	373	3.175	2.032	2.159	3.438	31.25	49.19	29.69
5	+135	393	7.620	6.350	5.969	8.486	14.88	17.88	7.25
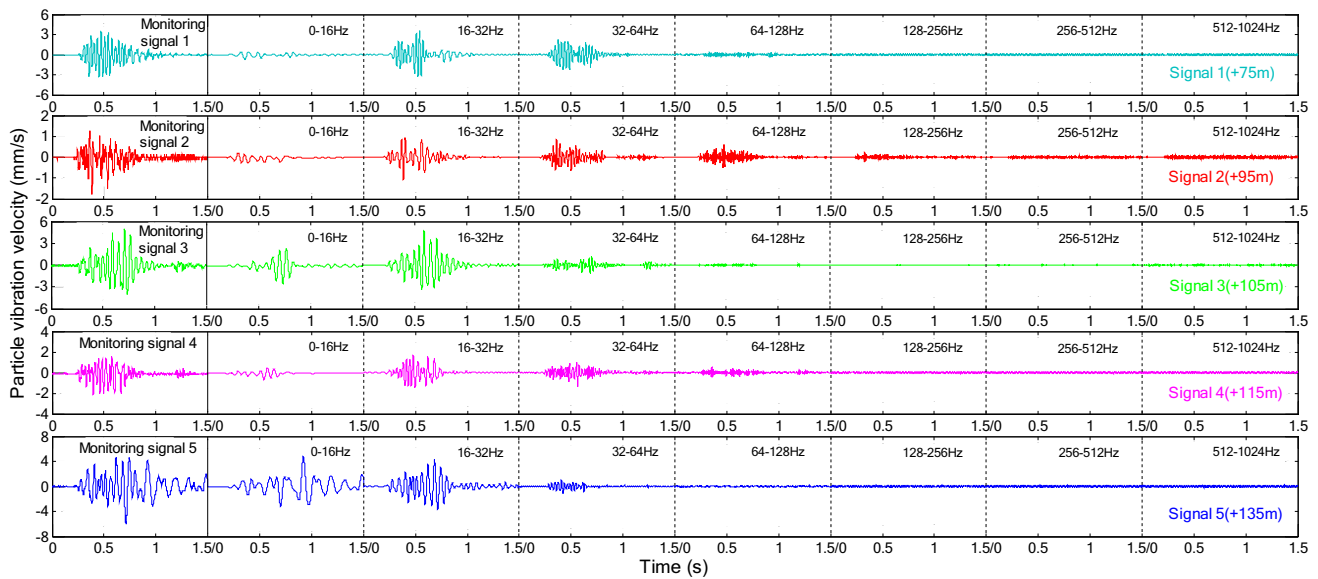
Fig. 6 Original vibration waveform and particle velocities time history curve of different frequency bands

In this study, based on the Moyal Theorem (Li et al. 2009), the square of the two sides of Eq. (10) were obtained as follows:

$$\int_R |f(t)|^2 dt = \frac{1}{C_\psi} \int_R \frac{da}{a^2} \int_R \left| W_f(a,b) \right|^2 db \qquad (12)$$

Equation (12) shows that the integral of the square of the particle amplitude was proportional to its energy. Therefore, in Eq. (12), $\left| W_f(a,b) \right|^2 \Big/ a^2 C_\psi$ can be regarded as a function of energy density in (a,b), and $\left| W_f(a,b) \right|^2 \Delta a \Delta b \Big/ a^2 C_\psi$ can also be regarded as the energy centered on the scale a and time b, in which the scale interval is represented by Δa, and the time interval is indicated Δb. Therefore, Eq. (12) was rewritten as follows:

$$\int_R |f(t)|^2 dt = \int_R E(b) db \qquad (13)$$

$$E(b) = \frac{1}{C_\psi} \int_R \frac{1}{a^2} \left| W_f(a,b) \right|^2 da \qquad (14)$$

Since the scale a of the wavelet transform had corresponded to the frequency under certain conditions, Eq. (14) was used in this study to represent the distribution of the signal energy in all frequency bands over time. Then, by adjusting the upper and lower limits of Eq. (14) so that the integration interval was consistent with the frequency range of the analyzed signal, the energy value and the percentage of the signal energy of any frequency band could be obtained. The relative energy could be written as follows:
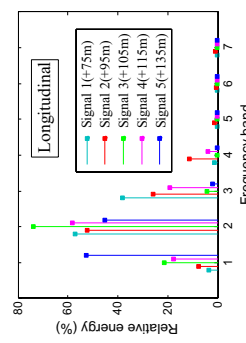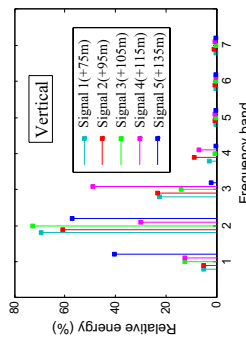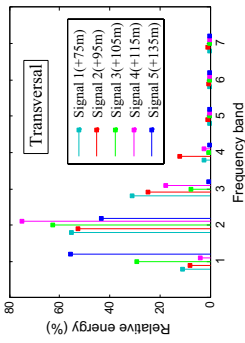
$$\eta_{(i,j)} = \frac{E_{(i,j)}}{E_{(0,1024)}} \times 100\% \ (0 < i < j < 1024) \qquad (15)$$

Table 3 presents the calculation results of the relative energy of each signal in the different frequency bands. To control a single elevation variable, signals 1, 3, and 5 are analyzed. It can be seen in Table 3 that the relative energies of Signal 1 (+75 m) and Signal 3 (+105 m) were mainly concentrated in the first to third frequency bands (frequency range: 0 to 64 Hz), and the relative energy sum of the other bands was less than 4%. Furthermore, the dominant vibration bands of Signal 1 (+75 m) and Signal 3 (+105 m) were also in the 16 to 32 Hz band. However, the relative energy distribution between the frequency bands was observed to exhibit a large change. It was found that when compared to Signal 1 (+75 m), the relative energy of Signal 3 (+105 m) had increased in the 0 to 16 Hz and 16 to 32 Hz bands, and had decreased in the 32–64 Hz and 64–128 Hz bands. The relative energy of Signal 5 (+135 m) was observed to be more than 97% in the first and second frequency bands (frequency range: 0–32 Hz). The main vibration frequency bands were in the 0–16 Hz and 16 to 32 Hz bands on the horizontal component and the vertical component, respectively. However, the relative energy on the vertical component had increased to 40.46% in the 0–16 Hz band. Due to the development of joints in the rock masses of the No. 2 (+95 m) and No. 4 (+115 m) benches, the relative energy of Signal 2 (+95 m) and Signal 4 (+115 m) in the 64–128 Hz band had ranged between 2.57% to 12.18%. The dominant vibration frequency band of Signal 2 (+95 m) was in the 16–32 Hz band on each of the components. However, the dominant vibration frequency bands of Signal 4 (+115 m)

Table 3 Relative energy distribution characteristics of vibration signals in different frequency bands

Vibration direction	points	Relative energy $\eta_{(i,j)}$ (%)							Relative energy of vibration signals in different frequency bands
		0–16 (Hz)	16–32 (Hz)	32–64 (Hz)	64–128 (Hz)	128–256 (Hz)	256–512 (Hz)	512–1024 (Hz)	
Transversal	1	11.04	55.22	30.97	2.53	0.10	0.05	0.09	
	2	7.88	52.70	24.70	12.18	0.94	0.50	1.09	
	3	29.17	62.59	7.50	0.42	0.06	0.09	0.18	
	4	4.05	75.02	17.79	2.57	0.14	0.13	0.30	
	5	55.64	43.53	0.65	0.05	0.04	0.04	0.06	
Vertical	1	4.88	69.23	22.57	2.89	0.26	0.07	0.12	
	2	5.03	60.99	23.27	8.76	0.60	0.41	0.95	
	3	12.23	72.86	13.93	0.50	0.05	0.08	0.15	
	4	12.34	30.04	48.76	7.06	0.72	0.34	0.74	
	5	40.46	57.23	2.02	0.08	0.06	0.06	0.09	
Longitudinal	1	3.52	57.10	37.98	1.15	0.10	0.05	0.10	
	2	7.79	52.12	25.70	11.38	1.45	0.51	1.04	
	3	21.44	74.00	4.29	0.14	0.03	0.04	0.07	
	4	17.79	58.34	19.27	3.81	0.24	0.19	0.37	
	5	52.55	45.09	2.01	0.09	0.08	0.08	0.10	

were in the 16–32 Hz and the 32–64 Hz band on the horizontal and the vertical component, respectively. It was observed that only the dominant vibration frequency band of Signal 4 had changed on the vertical component. In the current study, it was found that when Signal 2 (+95 m) was compared with Signal 1 (+75 m), and Signal 4 (+115 m) was compared with Signal 3 (+105 m), the relative energy had displayed a tendency to move to the higher frequency bands. These study's results indicated that with the increase in elevation, the dominant distribution frequency band of the relative energy of the blasting vibration signals had become narrower, and the dominant vibration frequency band had tended toward the low-frequency bands. However, it was observed that where the joints of the rock masses were developed, and the results were exactly the opposite.

Amplification coefficients of the PPV and vibration energy

The results detailed in "Comparative analysis of the PPV in the different frequency bands" and "Relative energy distribution characteristics of the vibration signals" indicated that the particle vibration intensities of the measured signals were mainly present in the first to third frequency bands (frequency range: 0–64 Hz). Yin et al. (2018) and Yuan et al. (2018) found that the main vibration frequency range of rock masses blasting is 0–50 Hz through on-site ground vibration monitoring, but there is no research on the amplification effect between the blasting vibration frequency bands in the jointed rock masses slope. Therefore, the PPV and energy amplification coefficients of the other signals were analyzed in this study in reference to that of Signal 1 (+75 m) in the
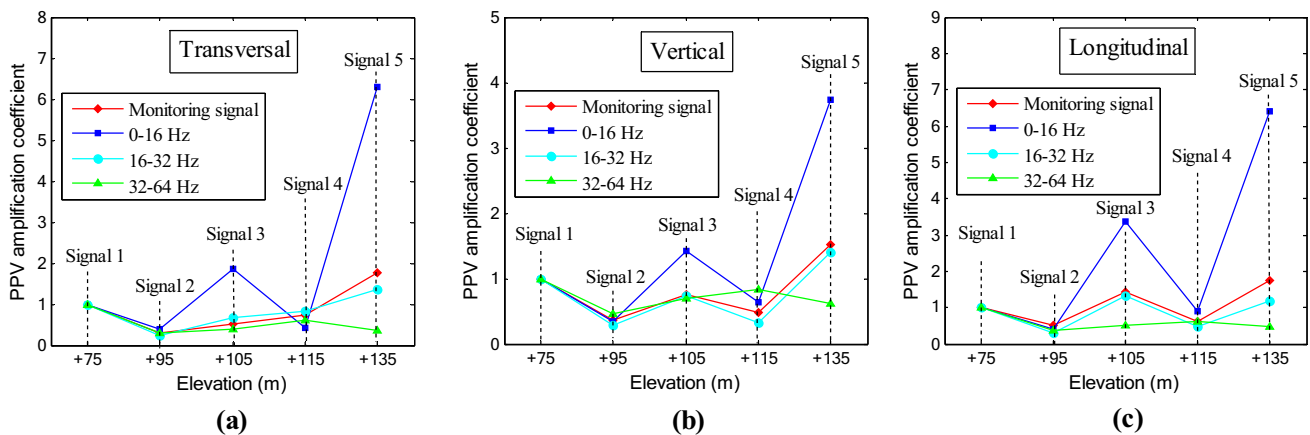

Fig. 7 Comparison of PPV amplification coefficient at different elevations: **a** transversal component; **b** vertical component; **c** longitudinal component
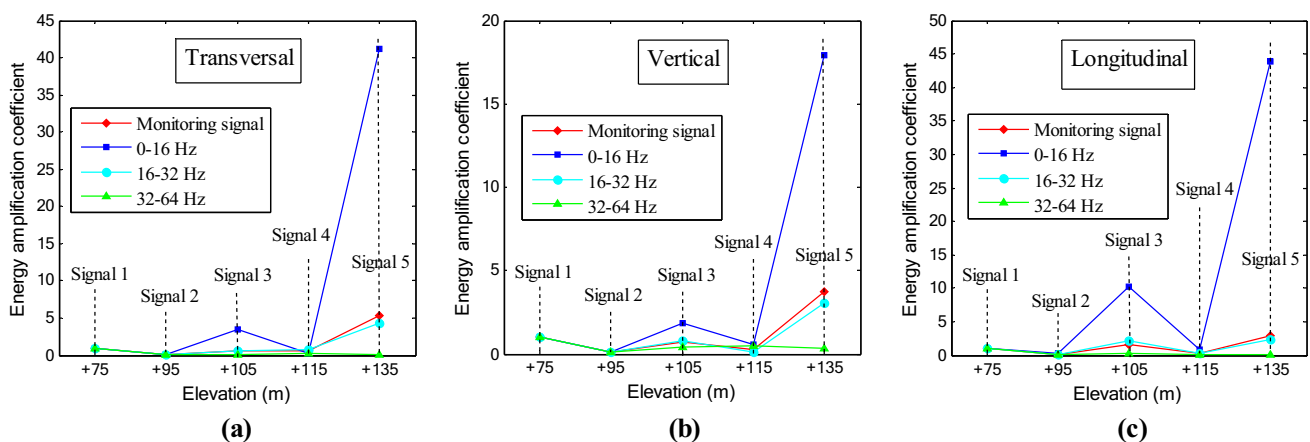

Fig. 8 Comparison of the amplification coefficient of vibration energy at different elevations: **a** transversal component; **b** vertical component; **c** longitudinal component
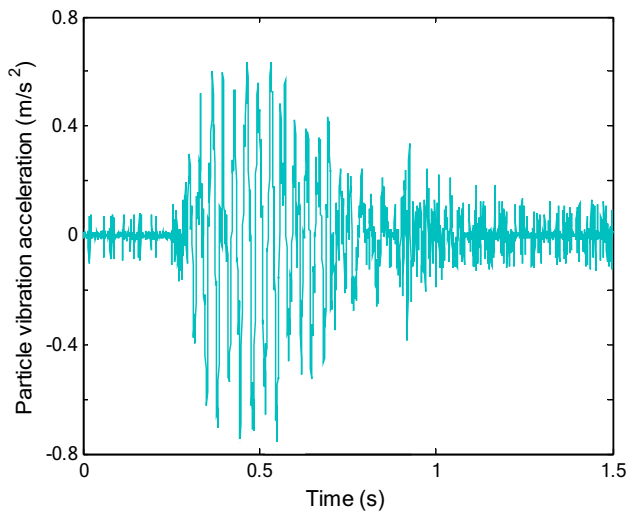
Fig. 9 Accelerations time history curve before denoising

total frequency bands (frequency range: 0–1024 Hz) and the first to third frequency bands (frequency range: 0–64 Hz).

As detailed in Figs. 7 and 8, there had been elevation amplification effects on the PPV and energy of the blasting vibration signals observed. However, the amplification coefficients between the different frequency bands differed, which was determined to be due to the changes in the vibration intensities and relative energy distribution characteristics of the signals between each of the frequency bands. The PPV and energy amplification effects of Signal 3 (+105 m) and Signal 5 (+135 m) were found to be the most obvious in the 0 to 16 Hz band, and their amplification coefficients were observed to be much larger than those of the total frequency band (frequency range: 0–1024 Hz). The vibration effects of Signal 3 (+105 m) and Signal 5 (+135 m) were attenuated in the 32–64 Hz band. These results indicated that during the blasting excavation activities of the high slope, the vibration intensities of the particles on the surface of the high-slope rock masses at long distances had gradually attenuated in the high-frequency part, and were mainly concentrated in the low-frequency part. These results may have caused the instability of the high slope which was characterized by a low natural frequency.

Signal 2 (+95 m) and Signal 4 (+115 m) had also displayed increases in elevation. However, the energy losses of the blasting seismic waves through the joints were found to be large. Therefore, the PPV and energy of the signals of each of the frequency bands were attenuated, and the degree of attenuation on each component was observed to be different. Signal 3 (+105 m) and Signal 5 (+135 m) had also passed through the propagation path of joint development. However, the signals were found to still show significant vibration amplification effects. The amplification coefficients were the largest on the longitudinal component;

second-highest on the transversal component; and smallest on the vertical component. Therefore, it was determined that the attenuation and amplification effects of the PPV and energy of the blasting vibration signals were the result of the influences of the slope elevation, along with the joints of the rock masses.

Blasting vibration response characteristics of the slope jointed rock masses

Through the aforementioned analysis results, it was determined in this study that the PPV and energy of signals had varied greatly in each of the frequency bands. The responses of the jointed rock masses to the blasting vibrations were determined by the external loads and inherent characteristics of the rock structures. In the present study, to analyze the response characteristics of the rock mass structures under the excitation of the blasting loads, a response spectrum calculation method was found to be effective. The response spectrum method (Lv 2015) was based on a single degree of freedom (SDOF) viscous damping system to simulate the vibration response characteristics of the real structures. Then, by inputting the vibration acceleration waveforms, the maximum vibration response amplitude of the single-mass system under natural frequency and damping conditions were successfully obtained. The ratio of the response spectrum value to the PPV represented the ordinate, which was referred to as the dynamic amplification coefficient. It should be noted that the response spectrum can also be seen as a method of analyzing the characteristics of the vibration spectrum.

It is known that blasting vibration signals include a large amount of noise. Liu et al. (2016) had previously denoised blasting vibration signals using wavelet threshold, empirical
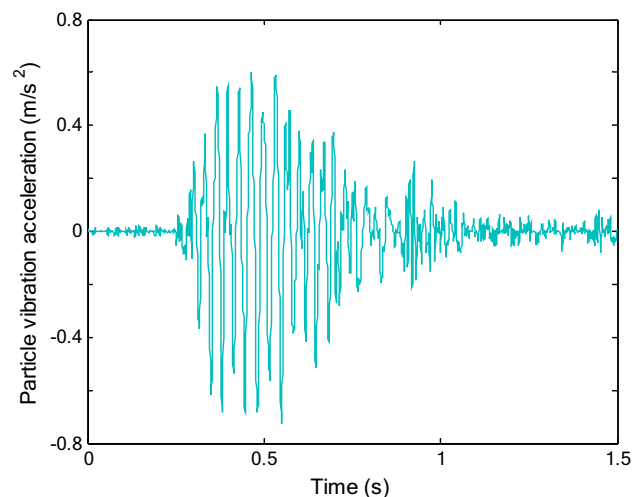

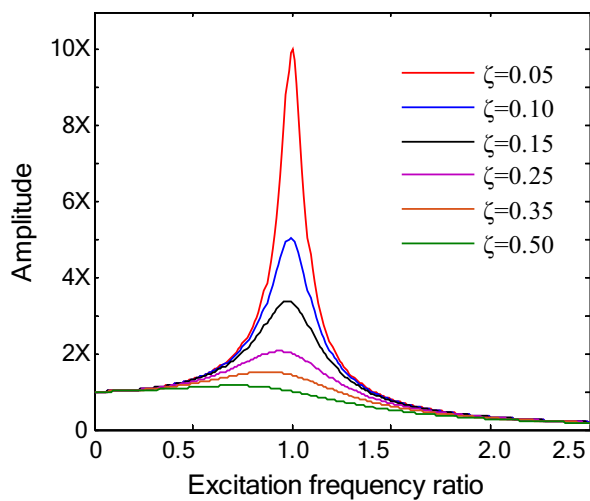Fig. 10 Accelerations time history curve after denoising

Fig. 11 Amplitude-frequency characteristic curves

mode decomposition (EMD), and ensemble empirical mode decomposition (EEMD) methods, respectively. The comparison analysis results showed that the denoising effects of the EEMD method were the most accurate. Therefore, in the current study, taking the waveform on the longitudinal component of Signal 1 (+ 75 m) as an example (Fig. 6), the measured particle velocities were differentiated, and the without denoised particle vibration accelerations are shown in Fig. 9. Then, an EEMD method was used for low-pass denoising to obtain the particle vibration accelerations, as detailed in Fig. 10.

Under the assumption that SDOF structures with different damping ratios are excited by a load with amplitude X (Basili et al. 2019), Fig. 11 illustrates the amplitude-frequency characteristic curves, and in which the excitation frequency ratio is equal to the excitation frequency divided by the natural frequency. It can be seen from Fig. 11 that the particle amplitudes were smaller with increases in the damping ratios under the excitation of the loads. It was also observed that, when the excitation frequency was closer
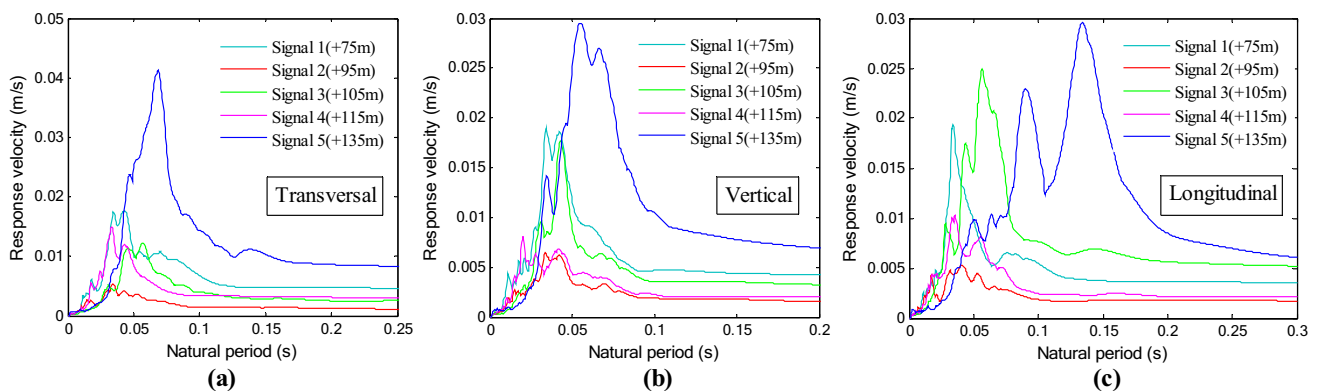

Fig.12 Velocity response spectrum: **a** transversal component; **b** vertical component; **c** longitudinal component
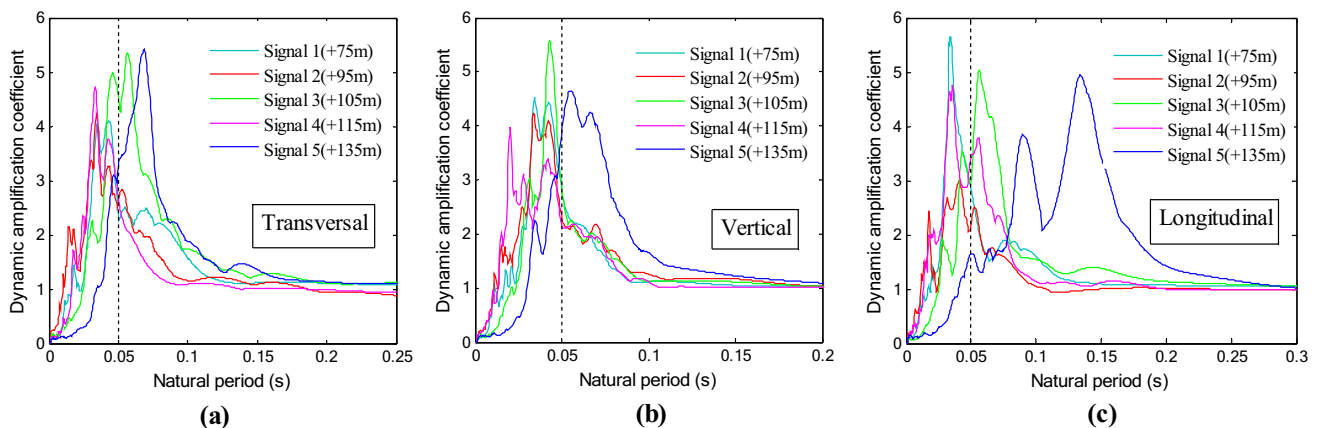

Fig. 13 The dynamic amplification coefficient of velocity response: **a** transversal component; **b** vertical component; **c** longitudinal component

to the natural frequency of the structure, then the particle amplitudes had increased sharply and formed a "prominent peak". That is to say, it was found to be more likely to result in the structure resonance. In the seismic calculations of actual engineering structures, the damping ratio $\xi = 0.05$ (Lv 2015) is generally taken. The calculated velocity response spectrum and the dynamic amplification coefficient of velocity response are shown in Figs. 12 and 13, in which the damping ratio $\xi = 0.05$ and denoised particle acceleration data were input.

As shown in Figs. 12 and 13, the response spectrum curves of the signals had multiple "prominent peaks", which indicated that the rock mass structure was a system composed of a group of substructures, and the substructures had different inherent characteristics. The response of the rock mass structure to the blasting seismic wave performance multi-mode and multi-modal characteristics, and the rock masses with joints development of No. 2 (+95 m) and No. 4 (+115 m) benches exhibit more obvious multi-mode and multi-modal characteristics, due to the greater number of "prominent peaks".

It was observed that as the elevation increased, the peaks of the velocity response spectrum of Signal 3 (+105 m) and Signal 5 (+135 m) had increased, and the dominant period had also increased. The number of the response spectrum "prominent peaks" in the low-frequency band was found to be higher, which had indicated that the signals had mainly displayed low-frequency band characteristics. Also, the dominant response frequency of the rock mass structure tended to be in the low-frequency range.

It was found in this study that, due to the influences of the joints, the number of the response spectrum "prominent peaks" of Signal 2 (+95 m) and Signal 4 (+115 m) in the high-frequency band were greater. The results indicated that the signals had mainly displayed high-frequency band characteristics, and the dominant response frequency of the rock mass structure had tended to be high frequency,

which had also validated the results detailed in "Relative energy distribution characteristics of the vibration signals" of this study. Furthermore, the multi-band phenomena were found to be more obvious, particularly when the response period was less than 0.05 s (i.e., the natural frequency was more than 20 Hz). When the natural frequency of the structure had differed greatly from the frequency of the blasting vibrations (for example, the natural frequency was less than 4 Hz or the natural period was more than 0.25 s), then the responses of the rock structure were observed to display only minimal changes.

Although the peaks of the velocity response spectrum had increased with the increasing elevation, and had attenuated into the rock masses with joints development, the peaks of the dynamic amplification coefficient of velocity response had displayed no obviously similar characteristics. The dynamic amplification coefficients of the jointed rock mass responses to the blasting vibrations were mainly determined by the inherent characteristics of the structure. The rock mass structure had shown selective amplification of blasting seismic waves in different directions at some of the frequencies. These results indicated that rock mass structure had different amplification effects on the frequency components of the blasting seismic waves, and the selective amplification effects on the blasting seismic waves in each direction had also varied.

Discussion

Based on the wave theory, it is generally believed that blasting seismic waves in jointed rock masses attenuate more quickly than homogeneous rock masses. Due to the fact that blasting seismic waves lose more energy through transmission and reflections at the joints of rock masses, the amplitudes and frequencies of the ground motion were reduced. However, this study's results showed that the dominant frequency bands of the blasting vibration signals of the
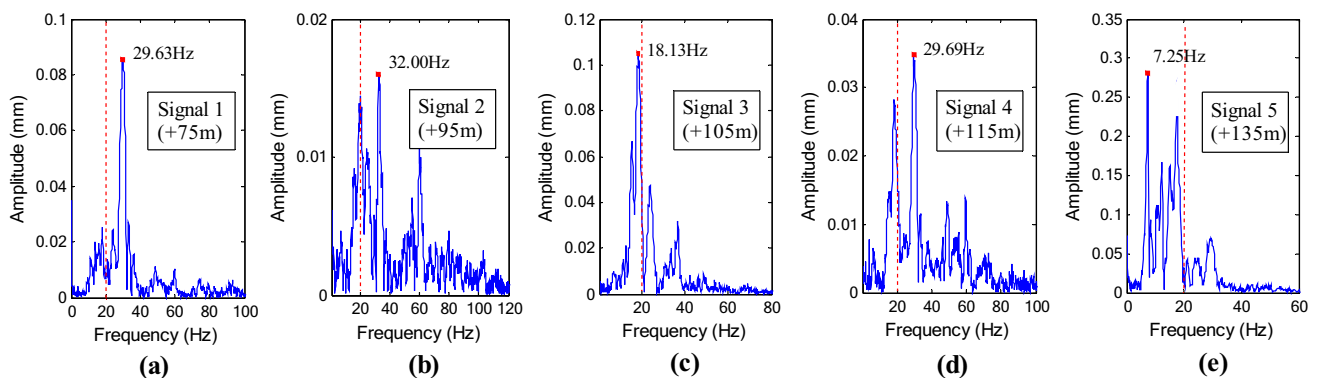

Fig. 14 Fourier spectrum of vibration signals on longitudinal component: **a** signal 1; **b** signal 2; **c** signal 3; **d** signal 4; **e** Signal 5

jointed rock masses tended to be the high-frequency bands, and some other related studies have drawn the same conclusions. Song et al. (2003) used the basic quality indexes and integrity coefficients of different rock masses to quantify the characteristics of the propagation medium, and found that the distribution ranges of the dominant frequency bands of detailed signal waveforms which were decomposed by the wavelet packet had increased as the integrity coefficients of the propagation medium had decreased. Also, Song et al. (2012) held that a single stress wave will produce many stress waves with phase differences after multiple reflections through joints in rock masses. It was observed that after the waveforms were superimposed, the frequencies had become higher, and the energy had moved to the high-frequency bands. Therefore, it was determined that according to the wave theory, the blasting vibration frequency band characteristics in rock masses with joints were not sufficiently explained.

In the current study, the high slope of the experimental site (Fig. 4) was composed of rock mass media with developed joints. From the perspective of the structural dynamics, it could be said that the jointed rock masses belonged to a multi-degree of freedom damped vibration system under blasting excitation conditions, and was characterized by multiple natural frequencies. The frequency boundary of 20 Hz (Fig. 14), and the frequency corresponding to the "prominent peak" of the Fourier Spectrum, were found to be in good agreement to that of the response spectrum "prominent peak" on the longitudinal component. Therefore, the multimode and multi-modal characteristics were more obvious in the rock masses with joints development, including the No. 2 (+95 m) and No. 4 (+115 m) benches.

Zhou et al. (2014) studied the multi-peak structures of blasting seismic wave spectra, as well as the differences in the attenuation rates between the high and low frequencies. The dominant frequencies of the blasting vibration signals were observed to be not strictly attenuated with the increase in the detonation distances. Also, mutations of the small-scale rock mass areas may occur during the attenuation processes. It was found that if the "prominent peak" of the Fourier Spectrum was expressed as a superior-frequency, then Signal 2 (+95 m) and Signal 4 (+115 m) tended to have superior frequencies which were greater than 20 Hz. Furthermore, when compared to the other signals, the frequency components of Signal 2 (+95 m) and Signal 4 (+115 m) were found to be more complex and the dominant frequencies were more likely to cause mutations. Due to the fact that the amplitudes of Signal 2 (+95 m) and Signal 4 (+115 m) were low, the amplitudes of the signals were normalized to solve the average frequency of the blasting seismic waves. The average frequency definition (Trivino et al. 2012) was as follows:
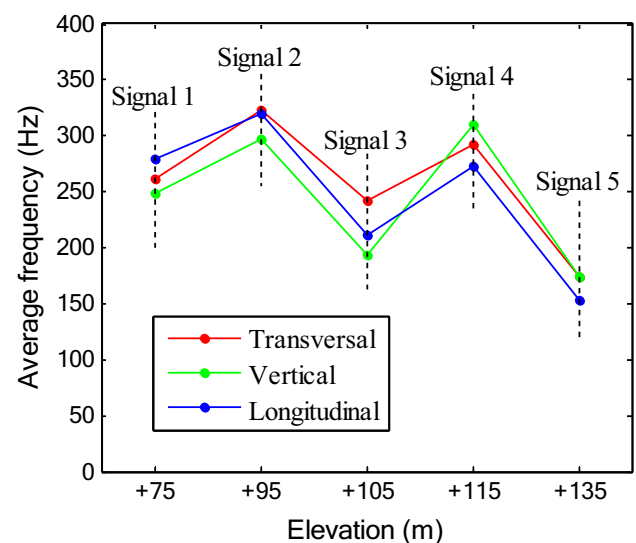

Fig. 15 The average frequency of vibration signals

$$\bar{f} = \sum_{i=1}^{n} \left(A_i f_i \right) \Big/ \sum_{i=1}^{n} A_i \tag{16}$$

where $\bar{f}$ represents the average frequency; f_i denotes each frequency in the Fourier Spectrum; and A_i is the amplitude associated with each frequency f_i.

It was observed in this study that as the elevation increased, the average frequencies of Signal 3 (+105 m) and Signal 5 (+135 m) had become reduced, while the average frequencies in the rock masses with joint development, such as those of Signal 2 (+95 m) and Signal 4 (+115 m) had increased (Fig. 15).

During the propagation of the blasting seismic waves into the jointed rock masses with slope, it was found that the whether or not the vibration responses of the particles would have amplification effects was mainly dependent on the relationships between the excitation frequencies and the natural frequencies of rock mass structures. Generally speaking, the natural frequencies of slope structures are small due to the large structural scale of the rock masses, and the lower stiffness value. However, some of the jointed rock masses of the exposed surfaces may have small mass scales and poor constraints, and the natural frequencies will be large. When the excitation frequencies are close to the natural frequencies of a slope, the response amplitudes of the particles will tend to increase, which may result in instability of the jointed rock masses. Therefore, the effects of the joints on the blasting vibration responses cannot be simply considered so as to reduce vibrations. The relationships between the blasting excitation frequencies and the natural frequencies of the jointed rock mass structures should also be explored, and the actual situations of the rock mass structural scales and

damping should be considered to determine the vibration responses of the particles. It was determined in this study that it was important and necessary to strengthen the support of small-scale rock masses with poor constraints, while also quickly handling dangerously unstable rock masses.

It should be pointed out that this study had focused on safety control and prediction of blasting vibrations for rock masses with joints and high slopes. However, the dips of the joint surfaces of the rock masses were ignored. It was believed that this study's results will potentially provide good references for future excavations of high rock slopes with joints.

Conclusions

The aim of this study was to safely control and predict the particle vibrations of rock masses with joints and high slope. Vibratory ground motions were measured during blasting excavation in open pit excavation, and the blasting vibration frequency band characteristics of rock masses with joints and high slope were studied through the wavelet transform and response spectrum method. The following conclusions were drawn from this study's results:

It was found that the effects of the joints on the blasting vibration responses could not be simply considered to effectively reduce vibrations. Therefore, the relationships between the blasting excitation frequencies and the natural frequencies of the jointed rock mass structures should be explored, and a vibration response theory should be used to characterize the blasting vibration intensities of the jointed rock masses.

It was determined that the rock mass structure was a system composed of a group of substructures. The jointed rock masses were found to have multiple substructures, and their multi-mode and multi-modal characteristics of the responses to the blasting seismic waves were more evident. The rock mass structure was also found to have different amplification effects on the frequency components of the blasting seismic waves. Furthermore, the selective amplification effects on the blasting seismic waves in each direction were also observed to be different.

It was observed that the PPV and energy of blasting vibrations had elevation amplification effects. However, the amplification coefficients between the different frequency bands had varied. It was found that with increase in elevation, the PPV and energy amplification effects of the particles were most obvious in the 0–16 Hz band. Meanwhile, they were found to be reduced in the 32–64 Hz band. The PPV and energy of the jointed rock masses in each of the frequency bands were found to be attenuated.

In the present study, it was observed that with increase in elevation, the dominant distribution frequency bands of the blasting vibration signals were low and narrow, and the average frequency had been reduced. However, in the joint development of the rock masses, the dominant distribution frequency bands of the signals were high and wide. Moreover, the multi-band phenomena of the signals were more obvious and the average frequency had been increased.

The results obtained in this study may contribute to the future blasting excavations of high rock slopes with joint fissures, in terms of applicability for guiding the blasting design, optimizing the blasting parameters, and ensuring the construction safety. However, this research may be less helpful in the excavation of rocky and soil mixed slopes or soil slopes.

Data availability The [TIFF of figure] data used to support the findings of this study are included within the article. Below are the data for the manuscript titled, "The characteristics of blasting vibration frequency bands in jointed rock mass slope".

Compliance with ethical standards

Conflict of interest The authors declare no conflict of interest regarding the publication of this paper.

References

Abdelwahed MF, Abdel-Fattah AK (2015) Scattering and intrinsic attenuation in Cairo metropolitan area using genetic algorithm. Soil Dyn Earthq Eng 69:93–102. https://doi.org/10.1016/j.soildyn.2014.10.020

Azizabadi HRM, Mansouri H, Fouche O (2014) Coupling of two methods, waveform superposition and numerical, to model blast vibration effect on slope stability in jointed rock masses. Comput Geotech 61:42–49. https://doi.org/10.1016/j.compgeo.2014.04.008

Bahrani A, Kaiser PK (2013) Strength degradation of non-persistently jointed rockmass. Int J Rock Mech Min 62:28–33. https://doi.org/10.1016/j.ijrmms.2013.03.013

Basili M, De Angelis M, Pietrosanti D (2019) Defective two adjacent single degree of freedom systems linked by spring-dashpot-inerter for vibration control. Eng Struct 188:480–492. https://doi.org/10.1016/j.engstruct.2019.03.030

Cao HX, Guo ZH (2016) Fundamental wavelet analysis. Springer, Beijing

Chen M, Lu WB, Li P, Liu MS, Zhou CB, Zhao G (2011) Elevation amplification effect of blasting vibration velocity in rock slope. Chin J Rock Mech Eng 30(11):2189–2195. https://doi.org/10.1007/s11629-011-1023-0

De A (2012) Numerical simulation of surface explosions over dry, cohesionless soil. Comput Geotech 43:72–79. https://doi.org/10.1016/j.compgeo.2012.02.007

Deng XF, Zhu JB, Chen SG, Zhao J (2012) Some fundamental issues and verification of 3DEC in modeling wave propagation in jointed rock masses. Rock Mech Rock Eng 45(5):943–951. https://doi.org/10.1007/s00603-012-0287-1

Fan SC, Jiao YY, Zhao J (2004) On modelling of incident boundary for wave propagation in jointed rock masses using discrete element method. Comput Geotech 31(1):57–66. https://doi.org/10.1016/j.compgeo.2003.11.002

Farrokhi M, Hamzehloo H, Rahimi H, Zadeh MA (2016) Separation of intrinsic and scattering attenuation in the crust of central and eastern Alborz region. Iran Phys Earth Planet Inter 253:88–96. https://doi.org/10.1016/j.pepi.2016.02.005

Forcellini D, Tanganelli M, Viti S (2018) Response site analyses of 3D homogeneous soil models. Emerg Sci J 2(5):238–250. https://doi.org/10.28991/esj-2018-01148

Ghasemi E, Ataei M, Hashemolhosseini H (2013) Development of a fuzzy model for predicting ground vibration caused by rock blasting in surface mining. J Vib Control 19(5):755–770. https://doi.org/10.1177/1077546312437002

Ghoraba S, Monjezi M, Talebi N, Armaghani DJ, Moghaddam MR (2016) Estimation of ground vibration produced by blasting operations through intelligent and empirical models. Environ Earth Sci 75(15):1137. https://doi.org/10.1007/s12665-016-5961-2

Graizer V (2009) Low-velocity zone and topography as a source of site amplification effect on Tarzana hill. California Soil Dyn Earthq Eng 29(2):324–332. https://doi.org/10.1016/j.soildyn.2008.03.005

Havenith HB, Vanini M, Jongmans D, Faccioli E (2003) Initiation of earthquake-induced slope failure: influence of topographical and other site specific amplification effects. J Seismol 7(3):397–412. https://doi.org/10.1023/A:1024534105559

Herrera G, Tomas R, Vicente F, Lopez-Sanchez JM, Mallorqui JJ, Mulas J (2010) Mapping ground movements in open pit mining areas using differential SAR interferometry. Int J Rock Mech Min 47(7):1114–1125. https://doi.org/10.1016/j.ijrmms.2010.07.006

Hosseini SA, Tavana A, Abdolahi SM, Darvishmaslak S (2019) Prediction of blast-induced ground vibrations in quarry sites: a comparison of GP, RSM and MARS. Soil Dyn Earthq Eng 119:118–129. https://doi.org/10.1016/j.soildyn.2019.01.011

Hu XL, Qu SJ, Jiang WL, Li H, Yang W, Huang HB, Hu GQ (2017) Attenuation law of blasting induced ground vibrations based on equivalent path. Explos Shock Wave 37(6):966–975

Hu YG, Liu MS, Wu XX, Zhao G, Li P (2018) Damage-vibration couple control of rock mass blasting for high rock slopes. Int J Rock Mech Min 103:137–144. https://doi.org/10.1016/j.ijrmms.2018.01.028

Huang D, Cui S, Li XQ (2019) Wavelet packet analysis of blasting vibration signal of mountain tunnel. Soil Dyn Earthq Eng 117:72–80. https://doi.org/10.1016/j.soildyn.2018.11.025

Jiang N, Zhou CB, Lu SW, Zhang Z (2017) Propagation and prediction of blasting vibration on slope in an open pit during underground mining. Tunn Undergr Space Technol 70:409–421. https://doi.org/10.1016/j.tust.2017.09.005

Kumar S, Singh P, Singh P, Shekhar C (2018) Estimation of scattering and intrinsic attenuation based on multiple lapse time window analysis in Sikkim Himalayan region, India. Phys Earth Planet Inter 284:1–9. https://doi.org/10.1016/j.pepi.2018.09.006

Li XB, Ling TH, Zhang YP (2009) Analysis of blast vibration singals-theories and methods. Springer, Beijing

Li YX, Zhu ZM, Li BX, Deng JH, Xie HP (2011) Study on the transmission and reflection of stress waves across joints. Int J Rock Mech Min 48(3):364–371. https://doi.org/10.1016/j.ijrmms.2011.01.002

Liu LS, Jiang JW, Zhou ZR, Liao MM (2016) Application of de-noising methods to blasting vibration signals. Nonferrous Met Sci Eng 7(3):107–112. https://doi.org/10.13264/j.cnki.ysjskx.2016.03.019

Lv XL (2015) Theory and examples of seismic design of building structures, 4th edn. Shanghai, China

Mohammadnejad M, Gholami R, Ramezanzadeh A, Jalali ME (2012) Prediction of blast-induced vibrations in limestone quarries using Support Vector Machine. J Vib Control 18(9):1322–1329. https://doi.org/10.1177/1077546311421052

Nakagawa S, Nihei KT, Myer LR (2000) Shear-induced conversion of seismic waves across single fractures. Int J Rock Mech Min 37(1–2):203–218. https://doi.org/10.1016/S1365-1609(99)00101-X

Nateghi R (2011) Prediction of ground vibration level induced by blasting at different rock units. Int J Rock Mech Min 48(6):899–908. https://doi.org/10.1016/j.ijrmms.2011.04.014

Nie L, Li ZC, Zhang M, Xu LN (2015) Deformation characteristics and mechanism of the landslide in West Open-Pit Mine, Fushun. China Arab J Geosci 8(7):4457–4468. https://doi.org/10.1007/s12517-014-1560-2

Park D, Jeon B, Jeon S (2009) A numerical study on the screening of blast-induced waves for reducing ground vibration. Rock Mech Rock Eng 42(3):449–473. https://doi.org/10.1007/s00603-008-0016-y

Rathore SS, Bhandari S (2007) Controlled fracture growth by blasting while protecting damages to remaining rock. Rock Mech Rock Eng 40(3):317–326. https://doi.org/10.1007/s00603-005-0080-5

Salvoni M, Dight PM (2016) Rock damage assessment in a large unstable slope from microseismic monitoring - MMG Century mine (Queensland, Australia) case study. Eng Geol 210:45–56. https://doi.org/10.1016/j.enggeo.2016.06.002

Sebastian R, Sitharam TG (2014) Transmission of elastic waves through a frictional boundary. Int J Rock Mech Min 66:84–90. https://doi.org/10.1016/j.ijrmms.2013.12.011

Shan NL, Cheng ZP, Liu YZ (2006) Engineering Seismic Exploration. Springer, Beijing

Song GM, Zeng XW, Chen SR, Wu CS (2003) Effect of propagation medium property on time-frequency characteristics of blasting vibration with wavelet packets analysis. Eng Blast 9(1):64–68. https://doi.org/10.3969/j.issn.1006-7051.2003.01.012

Song QJ, Li HB, Li JR, Yao WS, Yang FW, Wang M (2012) Influence of stratification on attenuation law of blasting vibration. Chin J Rock Mech Eng 31(10):2103–2108. https://doi.org/10.3969/j.issn.1000-6915.2012.10.016

Torres VFN, Silveira LCC, Lopes PFT (2018) deLima HM (2018) Assessing and controlling of bench blasting-induced vibrations to minimize impacts to a neighboring community. J Clean Prod 187:514–524. https://doi.org/10.1016/j.jclepro.2018.03.210

Trivino LF, Mohanty B, Milkereit B (2012) Seismic waveforms from explosive sources located in boreholes and initiated in different directions. J Appl Geophys 87:81–93. https://doi.org/10.1016/j.jappgeo.2012.09.004

Tuckey Z, Stead D (2016) Improvements to field and remote sensing methods for mapping discontinuity persistence and intact rock bridges in rock slopes. Eng Geol 208:136–153. https://doi.org/10.1016/j.enggeo.2016.05.001

Wang EH, Shukla A (2010) Analytical and experimental evaluation of energies during shock wave loading. Int J Impact Eng 37(12):1188–1196. https://doi.org/10.1016/j.ijimpeng.2010.07.003

Wang YP, Xiong LX (2020) Numerical analysis of the influence of bolt set on the shear resistance of jointed rock masses. Civ Eng J 6(6):1039–1055. https://doi.org/10.28991/cej-2020-03091527

Wu RS, Aki K (1988) Multiple scattering and energy transfer of seismic waves—separation of scattering effect from intrinsic attenuation II. Application of the theory to Hindu Kush region. Pure Appl Geophys 128:49–80. https://doi.org/10.1007/BF01772590

Wu YK, Hao H, Zhou YX, Chong K (1988) Propagation characteristics of blast-induced shock waves in a jointed rock mass. Soil Dyn Earthq Eng 17(6):407–412. https://doi.org/10.1016/S0267-7261(98)00030-X

Xu NX, Zhang JY, Tian H, Mei G, Ge Q (2016) Discrete element modeling of strata and surface movement induced by mining under open-pit final slope. Int J Rock Mech Min 88:61–76. https://doi.org/10.1016/j.ijrmms.2016.07.006

Xue XH, Yang XG (2014) Predicting blast-induced ground vibration using general regression neural network. J Vib Control 20(10):1512–1519. https://doi.org/10.1177/1077546312474680

Xue F, Zhang MX (2020) Stability of excavation face on shield tunnel undercrossing existing tunnel. Geotech Res 7(2):1–8. https://doi.org/10.1680/jgere.19.00027

Yang JH, Lu WB, Jiang QH, Yao C, Zhou CB (2016) Frequency comparison of blast-induced vibration per delay for the full-face millisecond delay blasting in underground opening excavation. Tunn Undergr Space Technol 51:189–201. https://doi.org/10.1016/j.tust.2015.10.036

Yin ZQ, Hu ZX, Wei ZD, Zhao GM, Ma HF, Zhuo Z (2018) Feng, RM (2018) Assessment of blasting-induced ground vibration in an open-Pit mine under different rock properties. Adv Civ Eng 6:1–10. https://doi.org/10.1155/2018/4603687

Yongping Copper Mine Geology Department (2012) Report on geological rock sample data of Yongping Copper Mine. Yongping Copper Mine of Jiangxi Copper Group, Jiangxi

Yuan HP, Liu XL, Liu Y, Bian HB, Chen W, Wang YX (2018) Analysis of acoustic wave frequency spectrum characters of rock mass under blasting damage based on the HHT method. Adv Civ Eng 3:1–8. https://doi.org/10.1155/2018/9207476

Zhang N, Wang WH, Yang ZQ, Zhang JN (2018) Numerical simulation on the stability of surrounding rock of horizontal rock strata in the tunnel. Civ Eng J 3(12):1189. https://doi.org/10.28991/cej-030948

Zhao XB, Zhao J, Cai JG, Hefny AM (2008) UDEC modelling on wave propagation across fractured rock masses. Comput Geotech 35(1):97–104. https://doi.org/10.1016/j.compgeo.2007.01.001

Zhou JR, Lu WB, Zhang L, Chen M, Yan P (2014) Attenuation of vibration frequency during propagation of blasting seismic wave. Chin J Rock Mech Eng 33(11):2171–2178. https://doi.org/10.13722/j.cnki.jrme.2014.11.002

Zhou J, Shi XZ, Li XB (2016) Utilizing gradient boosted machine for the prediction of damage to residential structures owing to blasting vibrations of open pit mining. J Vib Control 22(19):3986–3997. https://doi.org/10.1177/1077546314568172